Analysis of terahertz waveguide modes in continuous wavelet domain

Jianqiang Gu (谷建强)*, Zhen Tian (田 震), Qirong Xing (邢岐荣), Changlei Wang (王昌雷), Yanfeng Li (栗岩锋), Feng Liu (刘 丰), Lu Chai (柴 路), and Chingyue Wang (王清月)

Center for Terahertz Waves and Ultrafast Laser Laboratory, College of Precision Instrument and Optoelectronics Engineering, Key Laboratory of Opto-Electronics Information and Technical Science (Ministry of Education), Tianjin University, Tianjin 300072, China

**E-mail: gujianqiang@gmail.com*

Received June 1, 2010

Conventional analytical methods in the wavelet domain are used to present an analysis of terahertz (THz) waveguide modes. To obtain THz radiation pulses passing through a waveguide, we build a simple experimental system with a 5-mm-long, 230-μm-inner-diameter stainless steel waveguide. The single-mode guided signal from the experiments and the multi-mode signal of a similar THz waveguide reported in the literature are analyzed using the continuous wavelet transform (CWT). The results demonstrate that analyzing THz waveguide modes in the wavelet domain not only possesses all the functionality of the traditional THz time-domain spectroscopy (TDS) data processing but also has the ability to unscramble quantitatively and intuitively detailed information about the target samples, such as mode type, cut-off frequency, amplitude distinction, and group velocity.

OCIS codes: 300.6495, 230.7370.
doi: 10.3788/COL20100811.1057.

Terahertz (THz) science and technology has attracted tremendous attention in the last 20 years[1]. Among the THz techniques, THz time-domain spectroscopy (THz-TDS)[2] is a landmark detection modality by which the phase and amplitude of THz radiation can be obtained simultaneously. THz-TDS has opened up its applications in various fields, such as spectroscopy[3,4], imaging[5,6], biology[7], photonics[8], and communications. As a key component of many applications, THz waveguides have been widely studied. Various THz waveguides have been proposed, such as rigid hollow metallic waveguides[9], metal wires[10,11], solid core transparent dielectrics[12], hollow polycarbonate metal waveguides[13], hollow dielectric waveguides[14], plastic photonic crystal fibers[15,16], and metamaterial waveguides[17]. These waveguides are characterized by analyzing the transmitting signals, which are measured using THz-TDS, in virtual of classical waveguide theory[9], band gap analysis[15,16], Sommerfeld wave theory[11], metamaterial theory[17], algorithmic research (ARX), and state-space models with optimal wavelet pre-filtering[18].

In recent years, an alternative method that processes THz pulses with wavelet transform has been investigated in both the time and frequency domains[19,20]. In many applications, such as noise removal[18], data compression[21], tomography[22], and classification of THz spectra[23,24], wavelet transform outperforms most traditional techniques. However, until now, the use of wavelet transform to analyze THz-TDS-measured signals from a waveguide has not been adequately discussed. Although utilizing wavelets to analyze mode problems and waveguides has been reported in optical frequencies[25,26], it still remains attractive in the THz regime. In this letter, we utilize the continuous wavelet transform (CWT) to analyze time-resolved THz pulses emerging from some metallic cylindrical waveguides. The results show that quantitative and detailed information about the propagating waveguide modes can be visualized intuitively.

To obtain a nearly single-mode signal through a waveguide, we built a modified THz-TDS system with a 5-mm-long, 230-μm-inner-diameter stainless steel waveguide described in detail in our previous work[27]. The experimental setup is schematized in Fig. 1. Pulses of 50 fs at 810 nm with a 100-MHz repetition rate were split into a pump beam and a probe beam. The pump beam (200 mW) was focused using a 5-cm focus lens onto a <110> cut ZnTe THz emitter (1-mm thick), whereas the other beam was focused on the same ZnTe type, which acted as the detector. The waveguide was made from a commercial pinhead. The entrance of the waveguide perfectly matched the spot of the pump beam on the rear face of the emitter, allowing efficient coupling of the THz wave into the waveguide. The THz radiation transmitting through the sample was collected and collimated by two off-axis parabolic mirrors and measured by the other <110> cut ZnTe crystal based on the Pockels effect. The reference signal was measured when the emitter was placed at the focus of the parabolic collection mirror in the absence of the waveguide.

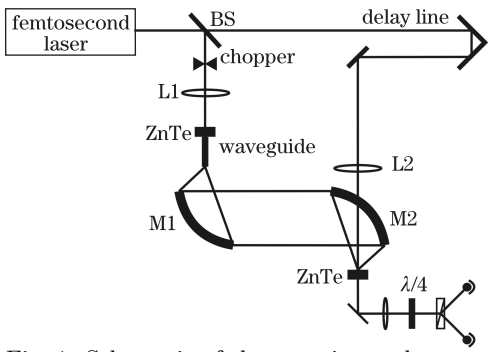

Fig. 1. Schematic of the experimental setup.

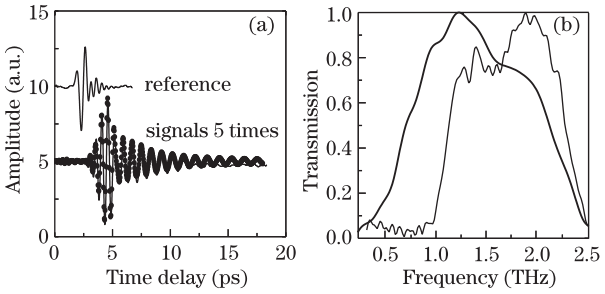

Fig. 2. (a) Temporal signal (thin solid line) passing through the waveguide. The reference signal is represented by the thick solid line. The dotted line is the simulation based on TE_{11} mode assumption. (b) Spectrum of the signal (thin solid line) and its reference.

Figure 2 shows the THz radiation pulse transmitting through the sample and its corresponding amplitude spectrum (thin lines) in comparison with that of the reference signal (thick lines). Compared with the reference, the signal from the waveguide has a temporal stretch of ~10 ps, with a higher frequency foreside and a slower oscillation at the rear end, which is a strong negative-chirped feature. The spectrum of the waveguide signal shown in Fig. 2(b) has a relatively sharp edge at the lower frequency of 0.76 THz compared with the reference spectrum. The dotted line in Fig. 2(a) is the theoretically calculated result based on the TE_{11} mode, which is usually the main mode in a circular waveguide. It fits the received signal curve reasonably well. In the following, we will show that in using a CWT process, the mode that plays the most important role in the waveguide can be confirmed.

Among the various mother wavelets, we chose the Gabor wavelet to analyze both the reference signal and the pulses passing through the waveguide because of its smallest Heisenberg box[28]. The expression of the Gabor mother wavelet is

$$\psi(t) = \frac{1}{(\sigma^2\pi)^{1/4}} \exp\left(-\frac{t^2}{2\sigma^2}\right) \exp(\mathrm{i}\omega_0 t), \qquad (1)$$

where σ represents the interval in the Gaussian-shaped window on the time scale, and ω_0 is the center frequency of the wavelet. The product of σ and ω_0 is an important parameter called "shaping factor" and is expressed as

$$G_\mathrm{s} = \sigma\omega_0. \qquad (2)$$

G_s governs the time-frequency resolution of CWT. The larger the shaping factor, the higher the spectral resolution (but the lower the time resolution), and *vice versa*[29].

The coefficient obtained by CWT on a temporal signal $f(t)$ can be expressed as

$$\Psi(a,b) = \frac{1}{a}\int_{-\infty}^{+\infty} f(t)\,\overline{\psi\left(\frac{t-b}{a}\right)}\,\mathrm{d}t, \qquad (3)$$

where b is the delay of the wavelet, and a=ω_0/ω is the scale factor, which is larger for a wavelet with a lower center frequency. Figure 3(a) plots the CWT coefficient map

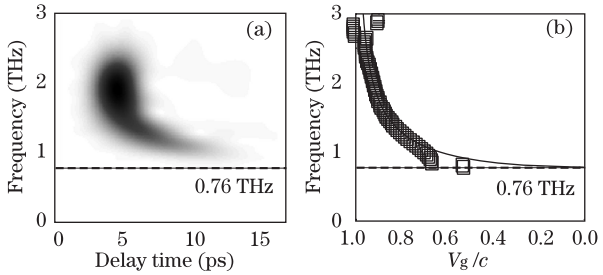

Fig. 3. Time-frequency characteristics of the THz radiation pulse emerging from the waveguide conducted by CWT with G_s=12.8. (a) A curved spectral band with an asymptote around 0.76 THz; (b) group velocity retrieval of the propagating waveguide mode, where the solid line is the theoretical result of the TE_{11} mode, and the squares are the experimental data obtained from the CWT results.

of the THz radiation pulse transmitting through the waveguide obtained in our experiment, where the vertical and horizontal axes denote the various center frequencies and the time delay of the wavelets, respectively. The gray scale represents the relative amplitude of the spectrum. In Fig. 3(a), the propagating waveguide mode is represented by a curved spectral band with an asymptote near 0.76 THz in the wavelet domain.

Wavelet transform simultaneously shows the time and frequency domain characteristics of the signals in one coefficient map, indicating that it can be utilized to analyze the group velocity of the propagating mode. The group delay B at a certain frequency ω_c, i.e., a certain scale factor a_c, is represented by the delay of the "related" wavelet that satisfies the condition $\Psi[a_\mathrm{c}, B(\omega_\mathrm{c})] = \max_b[\Psi(a_\mathrm{c}, b)]$. The group velocity of a certain mode in our case can be written as

$$V_\mathrm{g} = \frac{1}{\{[B_\mathrm{w}(\omega) - B_\mathrm{r}(\omega)]/L\} + 1/c}, \qquad (4)$$

where $B_\mathrm{w}(\omega)$ is the delay of the signal through the waveguide, $B_\mathrm{r}(\omega)$ is that of the reference signal, L is the length of the waveguide, and c is the velocity of light in vacuum. In Fig. 3(b), the squares are the group velocities retrieved at a shaping factor of 12.8. The solid line is the theoretical calculation based on the waveguide theory for TE_{11} mode, with a cut-off frequency of 0.76 THz for a 230-μm-diameter cylindrical waveguide. The retrieved and calculated results are in good accordance with each other in the most spectral part of our interest. The reasons for the deviation in the cut-off frequency and the group velocity near 0.76 THz are as follows. 1) The home-made waveguide we used is not perfectly fabricated, which must have caused some deviation from the calculated results based on the perfect and standard cylindrical waveguide assumption; 2) the precision of the CWT in the time domain decreases as the frequency goes down, which means it is correct in the main part of the signal spectrum only. Considering the consistency of the cut-off frequency, the group velocity, and the negative chirped property obtained from both the CWT and the waveguide theory, the spectral band shown in Fig. 3 corresponds to the waveguide mode TE_{11}. Compared with other methods, CWT gives an intuitive and simple method of presenting the asymptote line and the

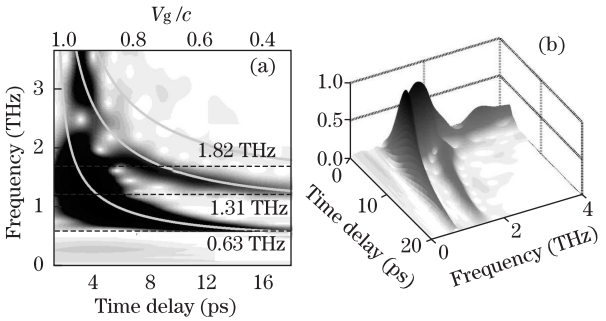

Fig. 4. (a) Time-frequency characteristics by CWT with G_s=12.8 for a THz pulse passing through the waveguide, as presented in Fig. 5 of Ref. [9]. The fine gray lines represent the theoretical results of group velocity for the dominant three modes. (b) Three-dimensional picture of the time-frequency characteristics of the signal.

dispersion type. CWT also has the capability to retrieve the group velocity of the mode.

To demonstrate the availability of analyzing THz waveguide modes in the wavelet domain further, we use our method to process a multi-mode case for the THz waveguide reported in Ref. [9]. We focus on the results shown in Fig. 5 of Ref. [9], which is a THz-TDS-measured THz radiation pulse and its corresponding amplitude spectrum through a 4-mm-long, 280-μm-diameter stainless steel waveguide. The incoming THz pulse shown in Fig. 2 of Ref. [9], which had a duration of ~1 ps and a corresponding amplitude spectrum from 0.1 to 4 THz, was stretched to a ~20-ps pulse with a negative chirp due to the strong group-velocity dispersion in the waveguide. The corresponding amplitude spectrum had a sharp cut-off at 0.63 THz, and the spectral oscillation appearing at approximately 1.5 THz implied the multi-mode propagation through the waveguide. We reconstruct the time domain data of the propagating waveguide signal and the incoming THz signal from Fig. 5 of Ref. [9] and show the CWT coefficient maps of the multi-mode pulse in Figs. 4(a) and (b). The shape of the map is apparently different from the single mode case, as shown in Fig. 4(a), which displays three bands curved with different trends having asymptotes near 0.63, 1.31, and 1.82 THz, respectively. This implies that the THz pulse transmitting through the waveguide contains three main propagating modes, i.e., TE_{11}, TM_{11}, and TE_{12} modes, respectively. This was proven in Ref. [9]. Compared with the Fourier transform method, which needs spectrum interference observation, mode coupling efficiency, and attenuation calculation based on waveguide theory, the CWT map provides an intuitive and easy method of mode identification. This mode-distinguishing capability of CWT arises from the fact that these three modes have different group velocities. We theoretically calculate the group velocity for these three modes in the air-filled 280-μm-diameter stainless steel waveguide shown as gray lines in Fig. 4(a). The trend of these three curved bands in the wavelet domain agrees well with the theoretical results of the group velocities of the waveguide modes, both in the curved trend and their asymptotes. In Fig. 4(b), we emphasize the relative contribution of these three different propagating modes, which is another main advantage of the wavelet analysis. The height and gray scale of each mode spectrum show that the TE_{11} mode is distributed mainly in the spectral region lower than 2.5 THz, whereas the TM_{11} mode is relatively stronger at 2.9 THz and above. There is also a very weak mode component TE_{12} in the waveguide, which is only predicted by the waveguide theory. The modulation of the band, which results from the mode spectrum interference, in the spectral region larger than 1.5 THz in Fig. 4(a), is in good accordance with that in Fig. 5(b) of Ref. [9]. The height directly reflected the different contributions of the three modes in the waveguide as determined together by the cut-off frequency, mode coupling efficiency, and attenuation.

In conclusion, we introduce CWT into the analysis of guided THz pulses transmitting through metallic THz waveguides. The single-mode signal from a 5-mm-long, 230-μm-inner-diameter stainless steel waveguide detected by THz-TDS and the multi-mode signal from the data reported in Ref. [9] are both analyzed in time-frequency space. The results demonstrate that CWT quantitatively and intuitively shows the detailed characteristics of the waveguide modes, such as mode type identification, cut-off frequency, mode coupling efficiency, attenuation, and group velocity retrieval. This simple but informative analysis method may find more applications in THz research.

We would like to thank D. Grischkowsky of Oklahoma State University for carefully reading the manuscript and for his constructive suggestions. We also appreciate the helpful discussions on wavelet transform provided to us by Y. Cao and L. Zhang of Tianjin University. This work was partly supported by the National "973" Project of China (No. 2007CB310408), the National Natural Science Foundation of China (No. 60578037), the National Natural Science Foundation of China-Rassian Foundation for Basic Research Program 2007–2008 (No. 60711120198), the Major Project of Tianjin Sci-Tech Support Program (No. 08ZCKFZC28000), the International Joint Program in Tianjin (No. 07ZCGHH01100), and the Project 985 Program of Tianjin University.

References

1. D. Dragoman and M. Dragoman, Prog. Quantum Electron. **28,** 1 (2004).
2. P. R. Smith, D. H. Auston, and M. C. Nuss, IEEE J. Quantum Electron. **24,** 255 (1988).
3. L. Lang, Q. Xing, S. Li, F. Mao, L. Chai, and Q. Wang, Chin. Opt. Lett. **2,** 677 (2004).
4. Q. Li, X. Chi, J. Shan, H. Zhang, and Q. Wang, Chinese J. Lasers (in Chinese) **35,** 756 (2008).
5. A. J. Fitzgerald, E. Berry, N. N. Zinovev, G. C. Walker, M. A. Smith, and J. M. Chamberlain, Phys. Med. Biol. **47,** R67 (2002).
6. Y. Wang, Z. Zhao, Z. Chen, L. Zhang, and K. Kang, Chin. Opt. Lett. **7,** 690 (2009).
7. B. Yu, F. Zeng, Y. Yang, Q. Xing, A. Chechin, X. Xin, I. Zeylikovich, and R. R. Alfano, Biophys. J. **86,** 1649 (2004).
8. Q. Xing, S. Li, Z. Tian, D. Liang, N. Zhang, L. Liang, L. Chai, and Q. Wang, Appl. Phys. Lett. **89,** 041107 (2006).
9. G. Gallot, S. P. Jamison, R. W. McGowan, and D. Grischkowsky, J. Opt. Soc. Am. B **17,** 851 (2000).

10. K. Wang and D. M. Mittleman, Nature **432,** 376 (2004).
11. T.-I. Jeon, J. Zhang, and D. Grischkowsky, Appl. Phys. Lett. **86,** 161904 (2005).
12. S. P. Jamision, R. W. McGowan, and D. Grischkowsky, Appl. Phys. Lett. **76,** 1987 (2000).
13. Y. Zhang, H. Zhang, Y. Geng, X. Tan, and J. Yao, Acta Phys. Sin. (in Chinese) **58,** 7030 (2009).
14. D. Chen and H. Chen, Opt. Express **18,** 3762 (2010).
15. H. Han, H. Park, M. Cho, and J. Kim, Appl. Phys. Lett. **80,** 2634 (2002).
16. J. Hu and H. Chen, Chinese J. Lasers (in Chinese) **35,** 567 (2008).
17. A. Ishikawa, S. Zhang, D. A. Genov, G. Bartal, and X. Zhang, Phys. Rev. Lett. **102,** 043904 (2009).
18. S. Hadjiloucas, R. K. H. Galvão, V. M. Becerra, J. W. Bowen, R. Martini, M. Brucherseifer, H. P. M. Pellemans, P. H. Bolívar, H. Kurz, and J. M. Chamberlain, IEEE Trans. Micro. Theory Tech. **52,** 2409 (2004).
19. Y. Deng, L. Lang, Q. Xing, S. Cao, J. Yu, T. Xu, J. Li, L. Xiong, Q. Wang, and Z. Zhang, Acta Phys. Sin. (in Chinese) **57,** 7747 (2008).
20. Y. Han, Q. Ge, C. Zhang, and L. Zhang, Computer Engineering and Applications (in Chinese) **44,** 241 (2008).
21. J. W. Handly, A. J. Fitzgerad, E. Berry, and R. D. Boyle, Phys. Med. Biol. **47,** 3885 (2002).
22. X. Yin, B. W.-H. Ng, B. Ferguson, and D. Abbott, Digital Signal Processing **19,** 750 (2009).
23. Y. Deng, Q. Xing, L. Lang, L. Chai, Q. Wang, and Z. Zhang, Acta Phys. Sin. (in Chinese) **54,** 5224 (2005).
24. Y. Chen, S. Huang, and E. Pickwell-MacPherson, Opt. Express **18,** 1177 (2010).
25. S. Barai and A. Sharma, J. Opt. Soc. Am. A **26,** 931 (2009).
26. M. I. Taroudakis and G. Tzagkarakis, J. Comput. Acoust. **12,** 175 (2004).
27. Q. Xing, L. Lang, Z. Tian, N. Zhang, S. Li, K. Wang, L. Chai, and Q. Wang, Opt. Commun. **267,** 422 (2006).
28. J.-C. Hong and Y. Y. Kim, Experimental Mechanics **44,** 387 (2004).
29. Y. Y. Kim, J. C. Hong, S. W. Han, I. K. Kim, and C. I. Park, in *Proceedings of IEEE Symposium on Ultrasonics* **2,** 1388 (2003).